Understanding the electrical, thermal and mechanical properties of LDPE-clay nanocomposites

Sundara Mallayan[1], Ramachandran Raja Prabhu[1], Belaguppa Manjunath Ashwin Desai[2], Ramachandran Velmurugan[3], Ramanujam Sarathi[2] ✉, Burjupati Nageshwar Rao[4]

[1]Department of Electrical and Electronics Engineering, B.S. Abdur Rahman University, Chennai-600 048, India
[2]Department of Electrical Engineering, Indian Institute of Technology Madras, Chennai-630 036, India
[3]Department of Aerospace Engineering, Indian Institute of Technology Madras, Chennai-630 036, India
[4]Central Power Research Institute, Bangalore-560 080, India
✉ E-mail: rsarathi@iitm.ac.in

The performance of low-density polyethylene (LDPE) clay nanocomposites was analysed. The inclusion of nano montmorillonite (MMT) clay in LDPE material has significantly increased the contact angle, corona ageing resistance, water droplet initiated corona inception voltage and surface discharge inception voltage of the composites. The surface charge decay rate of the samples significantly reduced on the inclusion of clay indicating modified trap distribution characteristics due to the inclusion of the filler. Dynamical mechanical analysis indicates increased storage modulus and reduced tan (δ) due to nanofillers inclusion. Laser-induced breakdown spectroscopy indicates that on inclusion of nanofillers the plasma temperature increases and crater depth decreases. In particular, increased discharge resistance, improved thermomechanical properties are observed with LDPE–MMT clay composites compared to pure LDPE.

1. Introduction: In recent times, high voltage direct current power transmission through underground cables have acquired considerable prominence, for transmitting bulk power. Cross-linked polyethylene (XLPE) material is used as an insulant extensively in underground cables. XLPE insulating material is susceptible to electrical discharges, electrical trees, space charge accumulation due to unreacted chemicals during the crosslinking process, which can cause early failure of cable insulation [1]. Low-density polyethylene (LDPE) is gaining importance because, it is a simple linear chain material, which is cost effective and there is a need to improve further, the dielectric properties of LDPE insulating material from an economic point of view [2].

In recent times, with the increased operating voltage with high ampacity, it is essential to develop a material which is space charge free, with good electrical properties and with high thermal conductivity. Poor thermal conductivity will lead to reduction in the life of the cable insulation. The enhanced electrical breakdown strength with high discharge resistance, space charge free insulating material with high thermal conductivity could be achieved by the addition of proper filler material to the insulating material [3].

Tanaka [4] carried out partial discharge resistance studies with LDPE–MgO nanocomposites by using IEC (b) electrode and have observed a reduction in the erosion of material by 36%. Alapati and Thomas [5] have observed increased treeing resistance by the inclusion of nanofillers in the LPDE material. Use of inorganic fillers like clay, silica and so on, improve the partial discharge resistance of the material significantly [6]. Eesaee *et al.*, have observed improved electrical breakdown strength with LDPE clay nanocomposites [7]. Also, clay-based LDPE composite has shown a very large increase in mechanical strength [8].

One of the major cause for the failure of insulating material is due to the occurrence of surface discharges. Also, the surface discharge inception voltage (SDIV) can provide an indication of the surface discharge resistance of the composites [9]. In recent times, with the increase in power electronic devices and a variety of loads, the supply voltage gets distorted with its total harmonic distortion (THD) which is as high as 40% [10].

In addition, the DC voltage profile's ripple content gets altered. The performance of the insulating material especially the surface discharge inception under the harmonic AC with different THD and with the DC voltages with different percentage of ripples, the database is scanty. To have the reliable design of insulation structure, it is essential to test the insulating material for surface discharges with near operating voltage profile.

Also to understand the impact of discharges on surface damage, one of the simplest method of analysis is by water droplet study. It allows one to correlate the hydrophobicity of the material and the amount of damage caused due to water droplet initiated discharges. Sarathi *et al.*, [11] have studied water droplet initiated discharges and have indicated that the amount of damage caused due to discharges is less with the nanocomposites.

Measurement of contact angle helps one to understand the hydrophobicity of the material [12]. It can quantitatively help one to determine the wettability of a solid surface by a liquid drop. Surface chemical heterogeneity and roughness are the key parameters that affect the wettability of a solid surface. It is essential to understand the characteristic changes that occur at the surface of the LDPE clay nanocomposites, by contact angle measurement.

One of the most conventional methods to understand the surface condition of the insulating material is by the measure of surface potential. The surface potential decay process study is vital to understand the possible changes in trap distribution and the charge transport process brought about by clay inclusion in the nanocomposites [13].

It is well known that inclusion of fillers in the polymer matrix can significantly change the viscoelastic property of the composites, which could be easily understood through dynamical mechanical analysis (DMA) of the material [14]. Thus it is essential to understand the storage modulus and tan (δ) of the nanofiller included LDPE material. In addition, it is essential to understand the composition of the material on the inclusion of nanofillers to the base material. In recent times, laser-induced breakdown spectroscopy (LIBS) which is a non-intrusive, non-destructive technique, is adopted to understand material composition and to analyse the level of ageing of the insulating material [15]. Such studies need to be carried out with nanoclay included LDPE material.

Having known all these facts, the following studies were carried out: (i) variation in contact angle of LDPE nanocomposite material

with different wt.% of clay, (ii) variation in SDIV with LDPE MMT clay nanocomposites under AC, harmonic AC voltages with different THDs and with DC voltages with different percentage of ripple contents, (iii) corona discharge inception voltage variation due to water droplet with LDPE nanocomposites, (iv) variation in surface potential and decay characteristics of the LDPE nanocomposites and to understand possible variation in trap distribution at different temperatures, (v) variation in viscoelastic property of LDPE clay nanocomposites through dynamic mechanical analysis, (vi) characteristic variation in LIBS spectra of LDPE clay nanocomposites and analysis of material properties.

2. Experimental studies

2.1. Experimental setup: Fig. 1 shows a schematic representation of the experimental setup used to determine water droplet initiated corona discharge inception voltage CIV and SDIV. The experimental setup can be sectionalised into the following parts: the high voltage source; the test electrodes; and the ultra-high frequency (UHF) sensor connected to the digital storage oscilloscope.

2.1.1. High voltage source: The required 50 Hz AC, high-frequency AC voltage, the harmonic AC voltage with different THDs and the DC voltages with different percentage of ripples were generated by use of Trek amplifier (Model 20/20C) in a current limit mode with input from a signal generator (Tektronix 3051C). The ripple DC was generated as in six-pulse full-bridge rectifier with different percentage of ripple. The voltage was applied to the test at the rate of 200 V/s. The AC voltage was measured using a capacitance divider and the DC voltage was measured using a resistance divider.

2.1.2. Test electrodes: The test electrode arrangement comprised of two stainless steel electrodes with their tip cut at 45° to enhance tangential electric field in the electrode gap (according to IEC 60112 [16]) set on 2 mm thick LDPE clay composite material. The electrodes were separated by a gap distance of 10 mm. One electrode was connected to the high voltage source through a resistance of 10 MΩ and the other electrode was connected to the ground. A 10 μl of deionised water was used as a droplet. For generating surface discharge activity, IEC (b) electrode was used. The test sample was placed between the top IEC (b) electrode and the ground plane electrode of 5 cm diameter (Fig. 1).

2.1.3. UHF sensor: In the present study, non-directional broadband UHF sensor was used by keeping the sensor at a distance of 20 cm from the test cell. The output of the UHF sensor connected to a high bandwidth digital storage oscilloscope (LeCroyWavepro 7300 A, 3.5 GHz bandwidth, operated at 20 GSa/s), to measure the shape of the signal generated by the sensor due to surface discharge activity.

2.2. Corona ageing: A 15 kV damped sinusoidal voltage of high frequency was used to generate corona. A sample of 4 cm × 4 cm dimension was kept on the ground plane electrode and the high voltage is connected to the top corona electrode. A gap of 1.5 mm was maintained between the top electrode and the sample surface. All the samples were exposed to corona ageing for 10 min, for understanding the impact of corona with the nanocomposite material.
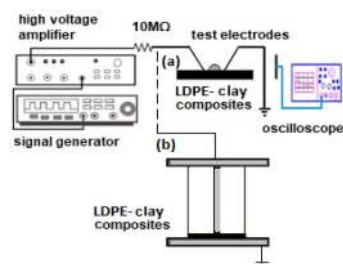
2.3. Surface potential measurement: Needle plane configuration was used to deposit charges on the LDPE composites by generating corona at 12 kV + DC and −DC. The surface potential was measured using an electrostatic voltmeter (Trek model 341B). The sensor responds to the charge deposited in 5 mm radius when it is placed 5 mm above the surface of the specimen [17]. To understand the impact of temperature of the specimen on surface potential decay characteristics, samples were placed on the hot plate, which was maintained at a required temperature and deposition of charges was carried as it was adopted at room temperature.

2.4. Laser-induced breakdown spectroscopy: When a pulsed laser source is directed on to the sample, electromagnetic radiations are emitted by the excited plasma elements. The specific wavelengths of the radiations can be considered as the fingerprints of the various elements which constitute the material. The experimental setup consists of a lens with a focal length of 25 cm, used to focus on Nd^{3+} YAG laser and a lens with 100 cm focal length used to capture the optical emission which is subsequently guided through multimode optical fibre with a core diameter of 400 μm, 0.22 NA to a spectrometer (ocean optics). A 1 s integration period was used to get the spectra. Fig. 2 shows a typical schematic representation of the LIBS setup.

2.5. Dynamic mechanical analysis: The dynamic mechanical properties of the pure LDPE and LDPE-clay nanocomposites were measured at different frequencies (1, 5, 10, and 20 Hz) and temperatures (span: −50 to 100°C) using DMA 242 D (NETZSCH) with a three-point bending fixture. The sample dimension was 50 mm × 11.5 mm × 2 mm. A sinusoidal strain was applied and the samples were heated at a rate of 3°C/min.

2.6. Sample preparation: Nanoclays are nanoparticles of layered mineral silicates. Depending on the chemical composition and nanoparticle morphology, nanoclays are organised into several classes. In the present study, organically modified nano dispersible layered silicate based on natural bentonite was used. The basic surface treatment is dimethyl, di(hydrogenated tallow) alkyl ammonium salt. The nanofiller is in off-white powdery form with a particle size <10 μm. The nanofiller of (1, 2, 3, 4 wt.%) has been weighed with respect to the polymer and added to a Banbury mixer, together with LDPE of 2.0 mass flow index and 0.4 gm of antioxidant IRGNOX as a thermal stabiliser. The temperature was maintained in the range from 155 to 160°C by water circulation to ensure a constant temperature. The mixing was carried out for a duration of about 10 min with an rpm of 30. The material is then transferred to a clean tray and the final temperature is measured. After cooling down to 40°C, the lump is ground into

Fig. 1 *Schematic representation of experimental setup for*
a Corona inception voltage
b Surface discharge inception voltage
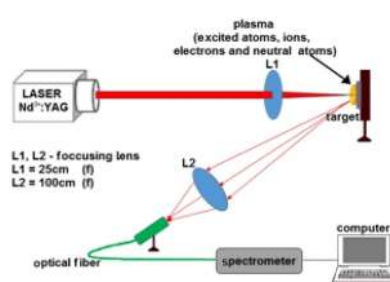
Fig. 2 *Schematic representation of the LIBS experimental setup*

small pieces. These pieces were further used to prepare 2 mm sheet on a compression moulding machine at 170°C.

3. Results and discussion

3.1. Contact angle measurement: Fig. 3a shows variation in contact angle of LDPE nanocomposites with different wt.% of clay and for corona treated specimens. Half angle method was used to obtain the contact angle. Five readings were taken on each side of the flat plate specimen, at different locations on the surface of the specimen and were averaged. Pure LDPE specimen has very low contact angle. On addition of nanoclay, a significant improvement in contact angle was observed with maximum contact angle for 3 wt.% sample. Increase in contact angle can be attributed due to good filler-matrix interaction. Good polymer-filler interaction implies, effective intercalation of chains of the polymer into the clay galleries, this preferential interaction of polymer chain with clay nanoparticles, reduces the overall free energy of the system [18]. Hence uniform dispersion of nanoparticle resulting in synergetic interaction of polymer with clay increases the contact angle of the system. There is a slight reduction with 4 wt.% sample possibly due to filler agglomeration.

Corona ageing can significantly alter the surface morphology of the polymeric insulating material. To understand the discharge resistance of the material, corona ageing was carried out. The contact angle was measured with a corona aged specimen and a significant reduction in contact angle was observed. However, reduction in contact angle after corona ageing is very large for pure LDPE, compared to LDPE clay composites.

3.2. Variation in CIV: Fig. 3b shows variation in water droplet initiated corona inception voltage (CIV) with different wt.% of clay in LDPE material. On application of voltage, water droplet placed between the electrodes undergoes polarisation and elongates along the axis of the electrodes. At the triple point formed by water, air and composite surface electric field intensification takes place and corona is initiated. Water droplet initiated CIV is determined based on the first UHF signal captured on the gradual increase of applied voltage. A nearly two-fold increase in CIV was observed with 3 wt.% composite. Higher CIV implies lower field intensification at normal operating voltage preventing discharge initiation. Water droplet initiated CIV depends on number of water droplets, the volume of water droplet, the contact angle of the water droplet (contact angle is a measure of the water droplet spread in the electrode gap) and also on the surface electric field [12]. Surface electric field depends on the relative permittivity of the composite.

As both volume and number of water droplets are held constant, CIV depends on contact angle and surface electric field. Increase in permittivity of the composite is prominent at higher concentration of nanofillers resulting in an exponential increase in the value of CIV with wt.% of clay in LDPE. When the weight percentage of nanofiller is increased above a certain limit, a reduction in contact angle is observed. A reduction in contact angle of water droplet indicates spread of water droplet in the electrode gap, which results in reduced effective electrode gap thereby reducing the corona to a much lower voltage.
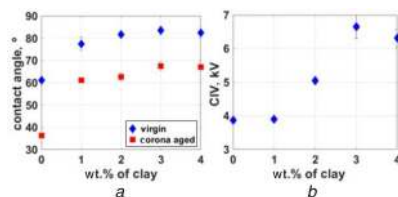
Fig. 3 *Variation in surface properties of composites with different wt%*
of clay
a Variation in contact angle with wt.% of clay in LDPE before and after corona aging
b Variation in CIV with wt.% of clay in LDPE

3.3. Variation in surface discharge inception voltage: An SDIV is determined based on the first UHF signal captured on the gradual increase of applied voltage. The SDIV values are an average of ten readings with maximum deviation observed to be <1%.

Table 1 shows the SDIV of LDPE nanocomposites under AC and harmonics AC voltage with different THDs. Surface discharge significantly depends on the peak value of the applied voltage. Fifth-order harmonic was found to have the least SDIV due to the fact that they have the highest peak factor. Under DC with an increase in ripple content, SDIV was found to decrease (Table 2). Overall independent of applied voltage profile significant increase in SDIV was observed with increase in clay wt.% in LDPE and 3 wt.% LDPE clay material has maximum SDIV. Further increase in wt.% of clay in LDPE has indicated to have lower SDIV. The cause could be due to agglomeration of filler resulting in weak spots for charge trapping and surface discharge. Higher SDIV of LDPE clay suggests increased surface discharge resistance of the material. Increased surface discharge resistance improves the tracking performance of the insulating material.

3.4. Surface potential measurement: The charge injected by the corona discharge process was deposited on top of the insulating material and the surface potential measurements were carried out using electrostatic voltmeter. On removal of charge deposition, the surface potential decays and this can be mathematically quantified as

$$V(t) = V_0 e^{-\lambda t} \qquad (1)$$

where λ is the decay rate and V_0 is the initial voltage measured.

Fig. 4 shows surface potential decay characteristics for different wt.% of clay in LDPE. Initial potential of LDPE nanocomposites with different percentage of clay was nearly the same. On the inclusion of clay particles, there is a significant increase in decay time. For 3 wt.% sample decay process was very slow indicating higher resistance to charge carrier mobility on the surface. Further with 4 wt.% decay time slightly reduced compared to 3 wt.% sample. Kumara *et al.* [19] have also observed a similar trend

Table 1 SDIV under AC and harmonic AC voltages with different THDs for LDPE clay composites

K	THD %	Peak factor	Surface discharge inception voltage, V_{rms}, kV				
			Pure LDPE	1 wt.%	2 wt.%	3 wt.%	4 wt.%
1	0	1.41	3.71	3.72	4.22	4.43	3.70
3	10	1.27	3.14	3.39	3.63	4.28	3.59
3	20	1.20	3.11	3.27	3.54	4.25	3.52
3	40	1.30	2.82	2.90	3.04	3.71	3.23
5	10	1.55	2.83	2.92	3.13	3.70	3.31
5	20	1.66	2.39	2.54	2.75	3.25	2.89
5	40	1.84	1.99	2.18	2.36	2.78	2.45
7	10	1.43	3.16	3.39	3.59	3.99	3.79
7	20	1.54	2.74	2.94	3.14	3.52	3.32
7	40	1.71	2.28	2.49	2.68	2.99	2.81

Table 2 SDIV under DC voltage with different ripple content for LDPE clay composites

Voltage with different % of ripple	Pure LDPE	1 wt.%	2 wt.%	3 wt.%	4 wt.%
+DC	14.95	15.06	15.84	17.58	16.32
+DC + 3%	14.64	14.52	15.18	16.38	15.06
+DC + 5%	13.32	13.26	14.04	15.18	13.98
−DC	15.18	15.66	16.32	18.12	16.92
−DC + 3%	14.64	15.12	15.78	16.92	15.66
−DC + 5%	13.86	13.92	14.76	15.84	14.52
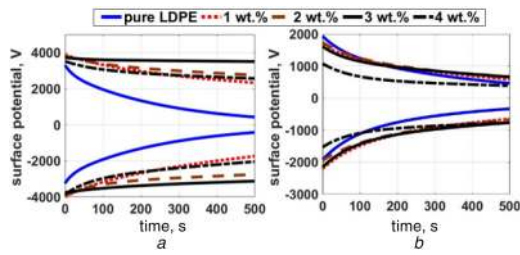
Fig. 4 *Surface potential decay characteristics of different clay–LDPE samples*
a 25°C and
b 60°C

Table 3 Initial voltage and decay rate for different samples

Polarity	+DC				−DC			
Sample	Initial voltage, kV		Decay rate λ, 10^{-3} s^{-1}		Initial voltage, kV		Decay rate λ, 10^{-3} s^{-1}	
	25°C	60°C	25°C	60°C	25°C	60°C	25°C	60°C
Pure	3.4	2.0	3.8	3.8	4	1.9	1.5	2.4
1 wt.%	3.9	1.7	0.6	1.7	4.1	2.2	1.3	1.6
2 wt.%	3.8	1.8	0.4	1.5	4.0	2	0.4	2.4
3 wt.%	3.7	1.6	0.2	2	3.8	2.2	0.3	1.1
4 wt.%	3.6	1.1	0.5	1.2	3.9	1.6	0.08	2.4

with LDPE Al$_2$O$_3$ nanocomposite. Table 3 shows the decay rate constant and initial potential for the LDPE clay nanocomposites. Similar characteristics have been observed, irrespective of the polarity of corona charging.

During operation, the cable insulation temperature is much higher than the room temperature depending on the local conditions. Hence, the surface potential variation was analysed at a higher temperature (60°C). It was observed that the initial potential on the surface decreases with increase in temperature. Also, the surface potential decay time shows an inverse relationship with temperature of the specimen in the range studied.

The surface trap distribution can be obtained from surface potential according to isothermal current decay theory [20]. The trap distribution is given by

$$N(E) = \frac{2\varepsilon_0\varepsilon_r}{qL^2kTf_0(E)}t\frac{dV}{dt} \qquad (2)$$

where q is electron charge, L is the sample thickness, T is ambient temperature, k is Boltzman constant and $f_0(E)$ is occupancy rate of initial electrons. The trap depth can be represented by

$$\Delta(E) = E_c - E_m = kT\ln(vt) \qquad (3)$$

where E_c and E_m represent the lowest level of the conduction band and time-dependent demarcation energy, respectively. Below E_m electrons are frozen in the traps [21].

Figs. 5 and 6 show the trap distribution of LDPE clay nanocomposites at 25 and 60°C, respectively. The trap distribution was calculated based on (2) and (3). It is observed from Fig. 5 that the trap energy level varies from 0.7 to 1 eV. The inclusion of nanofillers in the polymer matrix resulted in deeper traps with increased trap density for both positive and negative charges (Table 3). Increased trap density strongly correlates to higher initial charge with clay nanocomposites (Tables 3 and 4). Deeper trap level with composites strongly correlates with lower decay rate or higher detrapping time observed with clay composites (Tables 3 and 4). 3 wt.% sample has the highest trap level (Table 4) consequently has very low decay rate (Table 3). The interaction
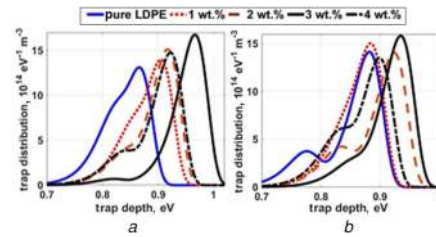
Fig. 5 *Trap distribution of Pure and LDPE composites at 25°C under*
a Positive corona charging and
b Negative corona charging
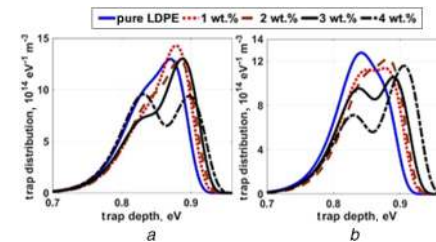
Fig. 6 *Trap distribution of Pure and LDPE composites at 60°C under*
a Positive corona charging and
b Negative corona charging

between intercalated molecular chains within the layered silicates may result in deeper trap levels.

It is observed from Fig. 6 that trap energy level varies from 0.7 to 0.95 eV. With the increase in sample temperature, trap distribution shifts to the left and peak trap density decreases. Higher temperature results in thermal activation and easy detrapping of the carriers [22]. Also, carrier mobility is enhanced at higher temperatures. As a result, prominent shallow traps are seen in trap distribution. Further, the influence of temperature was found to be more on the composites than on pure LDPE. Especially at high filler loading, where there is possible agglomeration, and less filler-matrix interaction effect of temperature is more (Tables 3 and 4).

3.5. Laser induced breakdown spectroscopy: Fig. 7 shows the LIBS spectra of pure and LDPE clay composites. In pure LDPE C, H and O peaks are observed. In clay composites, Na, Ca and Al peaks corresponding to MMT clay are observed along with the peaks that are observed in the virgin sample. The peaks of spectra are identified as per NIST database [23]. Laser spectra depend on various parameters like absorption coefficient, material hardness, melting point and so on. With 1 wt.% sample, Na peaks are not observed this is possibly due to lower filler content.

Based on the spectra, the temperature of the plasma formed by laser ablation can be calculated as per the Boltzmann Saha equation [24].

$$T_e = 1.44\frac{E_2 - E_1}{\ln\left[\frac{L_1*\lambda_1*A_2*g_2}{L_2*\lambda_2*A_1*g_1}\right]} \qquad (4)$$

where E_1 and E_2 are the excited energy levels, g_1 and g_2 are the statistical weights of excited energy levels 1 and 2, respectively, A_1 and A_2 are transition probabilities of states, I_1 and I_2 are the intensities of particular atomic species at λ_1 and λ_2 wavelengths, respectively and T_e is the plasma electron temperature under the condition of local thermodynamic equilibrium.

Laser ablation creates a crater of micrometre dimensions in the sample. Table 5 shows variation in the crater depth formed by laser ablation and plasma temperature (by (4)) are inversely related as shown in Table 5. Desai *et al.* [17] have indicated that plasma temperature of the material is directly proportional to the material hardness. A 3 wt.% sample has the highest plasma temperature

Table 4 Peak trap density and corresponding trap level for different samples

Polarity	+DC				−DC			
Sample	Trap depth, eV		Trap distribution, $10^{14}eV^{-1} m^{-3}$		Trap depth, eV		Trap distribution, $10^{14}eV^{-1} m^{-3}$	
	25°C	60°C	25°C	60°C	25°C	60°C	25°C	60°C
pure	0.88	0.87	13.1	12.9	0.88	0.84	14.1	12.8
1 wt.%	0.90	0.90	14	14.3	0.88	0.88	15.1	11.4
2 wt.%	0.92	0.88	15.1	12.9	0.92	0.88	14.1	12.2
3 wt.%	0.97	0.89	16.8	13.0	0.94	0.89	15.8	10.6
4 wt.%	0.92	0.83	14.8	9.6	0.9	0.91	13.5	11.6

Fig. 7 *LIBS spectra of LDPE clay nanocomposites*

Fig. 8 *Typical water droplet initiated discharge damage pictures of different LDPE clay composites*
a Pure LDPE
b 1 wt.%
c 2 wt.%
d 3 wt.% and
e 4 wt.%
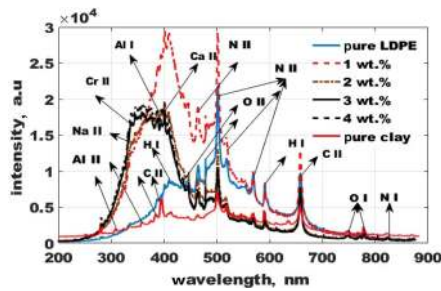
Table 5 Plasma temperature and crater depth and hardness for different samples

sample	Plasma temperature Te K	Crater depth, μm	Micro Vickers hardness
pure	10,216	85.93 ± 1	2.9 ± 0.2
1 wt.%	11,559	84.30 ± 1	3.1 ± 0.1
2 wt.%	12,979	84.10 ± 1	3.3 ± 0.1
3 wt.%	14,550	80.90 ± 1	3.8 ± 0.2
4 wt.%	10,185	102.91 ± 2	3.1 ± 0.3

Fig. 9 *Variation*
a storage modulus
b tan (δ) with temperature for pure and LDPE composites for 1 Hz frequency

and consequently the lower crater depth (Table 5) and the highest hardness (Table 5). Laser ablation can be treated as equivalent to localised thermal stress produced by electrical discharges in the insulating material. Lower crater depth clearly implies higher thermal resistance of the material. This strongly correlates to lower discharge damage observed with 3 wt.% sample (Fig. 8).

The inclusion of inorganic filler like clay increases the thermal stability and partial discharge resistance of the composite [3]. Uniform dispersion of nanoparticle in the matrix exposes very less amount of base matrix to any kind ageing. As a result crater with lower depth is formed for composites compared to pure LDPE. However, at higher fillers concentrations due to agglomeration of fillers weak spots are produced in the matrix. Hence, the 4 wt.% has higher crater depth and lower plasma temperature compared to pure LDPE. Thus LIBS can be used as a diagnostic tool to understand the condition of the insulating material.

3.6. Dynamic mechanical analysis: Polymers usually exhibit viscoelastic behaviour. The presence of fillers varies the entanglement and hence chain mobility of the polymer, therefore the viscoelastic property of the material can be significantly altered by the presence of the filler. Further, the interface regions can act as a region of stress transfers and can affect the stiffness of the material. Fig. 9a shows the variation of storage modulus of pure and LDPE composites with temperature. It is observed that storage modulus of composites is higher than that of pure LDPE and variation in storage modulus amongst different weight percentages in minimum. The increased storage modulus of the composites can
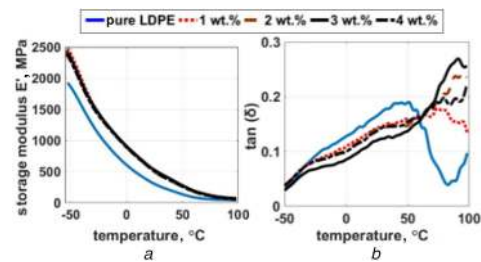
be attributed to the presence of filler with higher elastic modulus in the polymer matrix which provides higher stiffness to composite.

The overall effect of fillers on the composite's viscoelastic property can be analysed by tan (δ) of the composites. Fig. 9b shows the variation of tan (δ) of pure and LDPE composites with temperature. The tan (δ) is the measure of the ratio of the viscous modulus (loss modulus) to elastic modulus (storage modulus). With the increase in temperature polymer chain movement increases and storage modulus decreases. Further, with the increase in temperature chains start sliding over each other and viscous nature/loss modulus of matrix increases [25]. As a result of this simultaneous increase and decrease at a particular temperature peaking in tan (δ) is observed. This peak is around 50°C for pure LDPE and corresponds to ß relaxation of the composite.

It is observed that tan (δ) of pure LDPE is higher than composites and 3 wt.% sample has the least tan (δ). The presence of filler has two effects: increased stiffness due to filler's high modulus and increased viscous nature due to mesophasic interface. These two effects compete to form viscoelastic material. In the case of composites, stiffness factor dominates and hence composite have a lower tan (δ) compared to pure LDPE.

In Table 6, the glass transition temperature (T_g) corresponding to their loss modulus peaks. It is observed that clay composites have lower glass transition compared to pure sample. Also with the increase in frequency increase in glass transition is observed due to decreased molecular segmental motion with an increase in frequency (Table 6).

Table 6 Glass transition temperature (T_g) and activation energy (E_a) of pure and LDPE clay composites

Sample	E_a, kJ/mol	T_g, K (1 Hz)	T_g, K (5 Hz)	T_g, K (10 Hz)	T_g, K (20 Hz)
pure	312.14	247.57	249.22	251.47	252.22
1 wt.%	140.65	237.78	241.68	245.35	249.80
2 wt.%	172.57	241.26	246.93	245.11	247.83
3 wt.%	226.93	242.13	245.04	245.95	248.63
4 wt.%	183.01	240.29	246.01	245.09	252.22
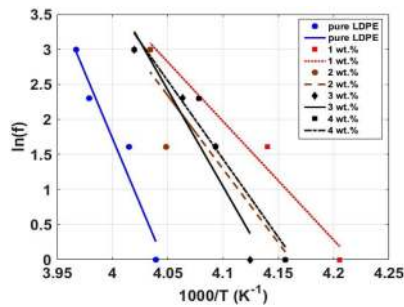
Fig. 10 *Arrhenius plot of ln(f) versus 1000/T for pure LDPE and LDPE-clay composites, markers indicate actual value and lines indicate estimated value*

The glass transition temperature, vibrational frequency and activation energy (E_a) are related by the Arrhenius equation shown as follows:

$$f = f_0 \exp\left[\frac{-E_a}{RT}\right] \quad (5)$$

where f is the applied vibrational frequency, R is gas constant, f_0 is constant of proportionality and E_a is the activation energy.

Fig. 10 shows the Arrhenius plot of ln(f) versus $1000/T$ for pure LDPE and LDPE-clay composites. It is observed that composites obey Arrhenius relation, hence the activation can be obtained from the slope of the Arrhenius plot.

Table 6 the glass transition temperature (T_g) and activation energy (E_a) of pure and LDPE clay. It is observed that clay composites have lower activation energy (E_a) compared to pure sample. Lower activation energy and lower glass transition temperature with composites compared to pure LDPE is possibly due to decreased entanglement due to the inclusion of filler particles in the matrix. Lower entanglement implies lower energy required for polymer chains to slide over each other. Amongst the composites, 3 wt.% sample has the highest activation energy and glass transition temperature. Further at higher fillers concentrations due to agglomeration of fillers weak spots are produced in the matrix. Where in these spots aid the chain sliding as result 4 wt.% sample has the least activation energy.

4. Conclusion: In the present study, we arrive at the following important conclusions: the inclusion of clay in the LDPE matrix resulted in improved discharge resistance. Increase in contact angle, water droplet initiated CIV and SDIV were observed with increase wt.% of clay in LDPE nanocomposites, with a reduction in performance above 3 wt.% of clay. The material exhibits improved resistance against corona ageing on the inclusion of filler. Surface potential decay was observed to be slow with composites, indicating increased resistance to surface charge mobility and significant modification of trap distribution on filler inclusion. Temperature's influence on trap distribution was more on the composites than on pure LDPE. DMA showed increased storage modulus and reduced tan (δ) on the inclusion of nanofillers. LIBS indicated that on the inclusion of nanofillers crater depth decreases which implies higher thermal resistance of the material.

5 References

[1] Dissado L.A., Fothergill J.C.: 'Electrical degradation and breakdown in polymers', in Stevens G.C. (ED.): 'IET materials and devices Series 9', vol. 27 (Peter Peregrinus Ltd, London, UK, 1992), pp. 117–143

[2] Chen X.R., Murdany D., Liu D.M., *ET AL.*: 'AC and DC pre-stressed electrical trees in LDPE and its aluminum oxide nanocomposites', *IEEE Trans. Dielectr. Electr. Insul.*, 2016, **23**, (3), pp. 1506–1514

[3] Tanaka T., Imai T.: 'Advanced nanodielectrics: fundamentals and applications' (CRC Press, USA, 2017)

[4] Tanaka T.: 'Dielectric nanocomposites with insulating properties', *IEEE Trans. Dielectr. Electr. Insul.*, 2005, **12**, pp. 914–928

[5] Alapati S., Thomas M.J.: 'Electrical treeing and the associated PD characteristics in LDPE nanocomposites', *IEEE Trans. Dielectr. Electr. Insul.*, 2012, **19**, (2), pp. 697–704

[6] Kozako M., Kuge S.I., Imai T., *ET AL.*: 'Surface erosion due to partial discharges on several kinds of epoxy nanocomposites'. Proc. of the Annual Report – Conf. on Electrical Insulation and Dielectric Phenomena (CEIDP '05), 2005, pp. 162–165

[7] Eesaee M., David E., Nicole R., *ET AL.*: 'Electrical breakdown properties of clay-based LDPE blends and nanocomposites', *J. Nanomater.*, 2018, **2018**, pp. 1–17

[8] Arunvisut S., Phummanee S., Somwangthararoj A.: 'Effect of clay on mechanical and gas barrier properties of blown film LDPE/clay nanocomposites', *J. Appl. Polym. Sci.*, 2007, **106**, pp. 2210–2217

[9] Sarathi R., Sahoo A., Chen Y., *ET AL.*: 'Understanding surface discharge activity with epoxy silicon carbide nanocomposites', *Polym. Eng. Sci.*, 2017, **57**, pp. 1349–1355

[10] Sonerud B., Bengtsson T., Blennow J., *ET AL.*: 'Dielectric heating in insulating materials subjected to voltage waveforms with high harmonic content', *IEEE Trans. Dielectr. Electr. Insul.*, 1995, **16**, (4), pp. 926–933

[11] Sarathi R., Harsha V.S., Vasa N.J., *ET AL.*: 'Water droplet initiated discharges on epoxy nanocomposites under DC voltages', *IEEE Trans. Dielectr. Electr. Insul.*, 2016, **23**, (3), pp. 1743–1752

[12] Lopes I.J.S., Jayaram S.H., Cherney E.A.: 'A study of partial discharges from water droplets on a silicone rubber insulating surface', *IEEE Trans. Dielectr. Electr. Insul.*, Nashville, USA, 2001, **8**, (2), pp. 262–268

[13] Molinie P.: 'A review of mechanisms and models accounting for surface potential decay', *IEEE Trans. Plasma Sci.*, 2012, **40**, (2), pp. 167–175

[14] Zhang H., Wei Y., Kang Z., *ET AL.*: 'Influence of partial substitution for carbon black with graphene oxide on dynamic properties of natural rubber composites', *IET Micro Nano Lett.*, 2017, **12**, (9), pp. 605–610

[15] Meyer L.H., Jayaram S.H., Cherney E.A.: 'A novel technique to evaluate the erosion resistance of silicone rubber composites for high voltage outdoor insulation using infrared laser erosion', *IEEE Trans. Dielectr. Electr. Insul.*, 2005, **12**, (6), pp. 1201–1208

[16] IEC publication, 60 112: 'Recommended method for determining the comparative tracking index of solid insulating material under the moist condition' (IEC, Geneva, Switzerland, 1972, 2nd edn.)

[17] Desai B.M.A., Mishra P., Vasa N.J., *ET AL.*: 'Understanding the performance of corona aged epoxy nano micro composites', *IET Micro Nano Lett.*, 2018, **13**, (9), pp. 1280–1285

[18] Rogers K., Takacs E., Thompson M.R.: 'Contact angle measurement of select compatibilizers for polymer-silicate layer nanocomposites', *Polym. Test.*, 2005, **24**, (4), pp. 423–427

[19] Kumara J.R.S.S, Serdyuk Y.V., Gubanski S.M.: 'Surface potential decay on LDPE and LDPE/Al$_2$O$_3$-nano-composites: measurements and modeling', *IEEE Trans. Dielectr. Electr. Insul.*, 2016, **23**, (6), pp. 3466–3475

[20] Simmons J.G.S., Tam M.C.: 'Theory of isothermal currents and the direct determination of trap parameters in semiconductors and insulators containing arbitrary trap distributions', *Phys. Rev. B*, 1973, **7**, (8), pp. 3706–3716

[21] Watson P.K.: 'The thermalization and trapping of electrons in polystyrene', *IEEE Trans. Dielectr. Electr. Insul.*, 1987, **EI-22**, (2), pp. 129–132

[22] Ziari Z., Mallem H., Sahli S.: 'Influence of the temperature on the surface potential decay of polymer films charged negatively by corona discharge under light radiation'. Proc. of 2014 Mediterranean Microwave Symp. (MMS 2014), Marrakech, 2014, pp. 1–4

[23] Sansonetti J.E., Martin W.C.: 'Handbook of basic atomic spectroscopic data', *J. Phys. Chem. Ref. Data*, 2005, **34**, pp. 1559–2259

[24] Descoeudres A., Hollenstein C., Demellayer R., *ET AL.*: 'Optical emission spectroscopy of electrical discharge machining plasma', *J. Phys. D., Appl. Phys.*, 2006, **37**, (6), pp. 875–882

[25] Menczel J.D., Prime R.B.: 'Thermal analysis of polymers: fundamentals and applications' (Wiley, USA, 2009)